

13. Fluid Sheets

13.1 Fluid Sheets: shape and stability

The dynamics of high-speed fluid sheets was first considered by *Savart (1833)* after his early work on electromagnetism with Biot, and was subsequently examined by *Rayleigh (1879)*, then in a series of papers by Taylor (*Proc. Roy. Soc., 1959*). They have recently received a great deal of attention owing to their relevance in a number of spray atomization processes. Such sheets may be generated from a variety of source conditions, for example, the collision of jets on rigid impactors, and jet-jet collisions. There is generally a curvature force acting on the sheet edge which acts to contain the fluid sheet. For a 2D (planar) sheet, the magnitude of this curvature force is given by

$$\mathbf{F}_c = \int_C \sigma (\nabla \cdot \mathbf{n}) \mathbf{n} dl \quad (13.1)$$

Using the first Frenet-Serret equation (Lecture 2, Appendix B),

$$(\nabla \cdot \mathbf{n}) \mathbf{n} = \frac{dt}{dl} \quad (13.2)$$

thus yields

$$\mathbf{F}_c = \int_C \sigma \frac{dt}{dl} dl = \sigma (\mathbf{t}_1 - \mathbf{t}_2) = 2\sigma \mathbf{x} \quad (13.3)$$

There is thus an effective force per unit length 2σ along the length of the sheet rim acting to contain the rim. We now consider how this result may be applied to compute sheet shapes for three distinct cases: i) a circular sheet, ii) a lenticular sheet with unstable rims, and iii) a lenticular sheet with stable rims.

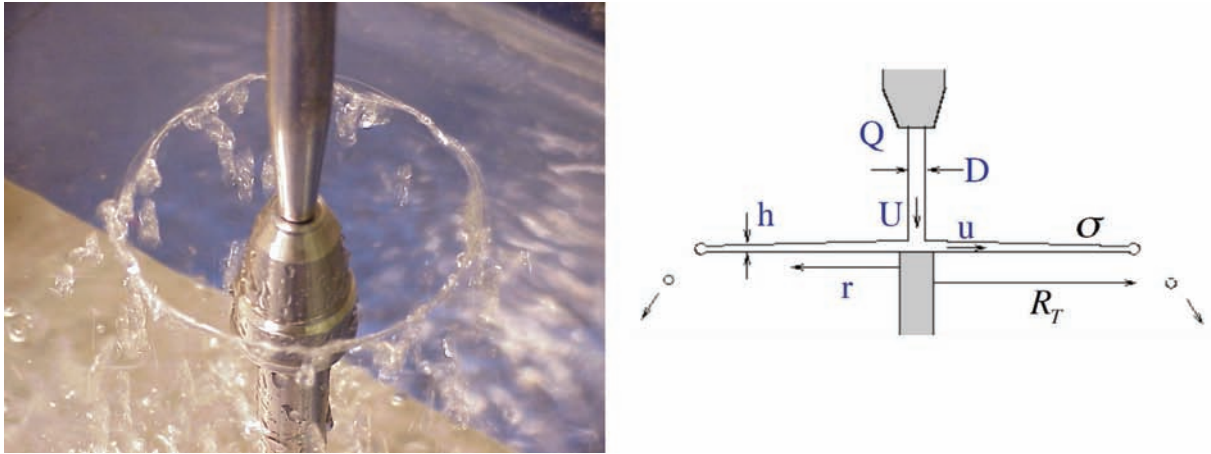


Figure 13.1: A circular fluid sheet generated by the impact of a water jet on a circular impactor. The impacting circle has a diameter of 1 cm.

13.2 Circular Sheet

We consider the geometry considered in Savart's original experiment. A vertical fluid jet strikes a small horizontal circular impactor. If the flow rate is sufficiently high that gravity does not influence the sheet shape, the fluid is ejected radially, giving rise to a circular free fluid sheet (Fig. 13.1).

For $We = \frac{\rho U^2 D}{\sigma} > 1000$, the circular sheet is subject to the flapping instability. We thus consider $We < 1000$, for which the sheet is stable. Scaling: $Re = \frac{UR}{\nu} \sim \frac{30 \cdot 10}{0.01} \sim 3 \cdot 10^4 \gg 1$. $Fr = \frac{U^2}{gR} \sim \frac{30^2}{10^3 \cdot 10} \sim 0.1$ so inertia dominates gravity.

The sheet radius is prescribed by a balance of radial forces; specifically, the inertial force must balance the curvature force:

$$\rho u^2 h = 2\sigma \quad (13.4)$$

Continuity requires that the sheet thickness h depend on the speed u , jet flux Q and radius r as

$$h(r) = \frac{Q}{2\pi r u} \sim \frac{1}{r} \quad (13.5)$$

Experiments (specifically, tracking of particles suspended within the sheet) indicate that the sheet speed u is independent of radius; consequently, the sheet thickness decreases as $1/r$. Substituting the form (13.5) for h into the force balance (13.4) yields the sheet radius, or so-called Taylor radius:

$$R_T = \frac{\rho Q u}{4\pi\sigma} \quad (13.6)$$

The sheet radius increases with source flux and sheet speed, but decreases with surface tension. We note that the fluid proceeds radially to the sheet edge, where it accumulates until going unstable via a modified Rayleigh-Plateau instability, often referred to as the Rayleigh-Plateau-Savart instability, as it was first observed on a sheet edge by Savart.

13.3 Lenticular sheets with unstable rims (Taylor 1960)

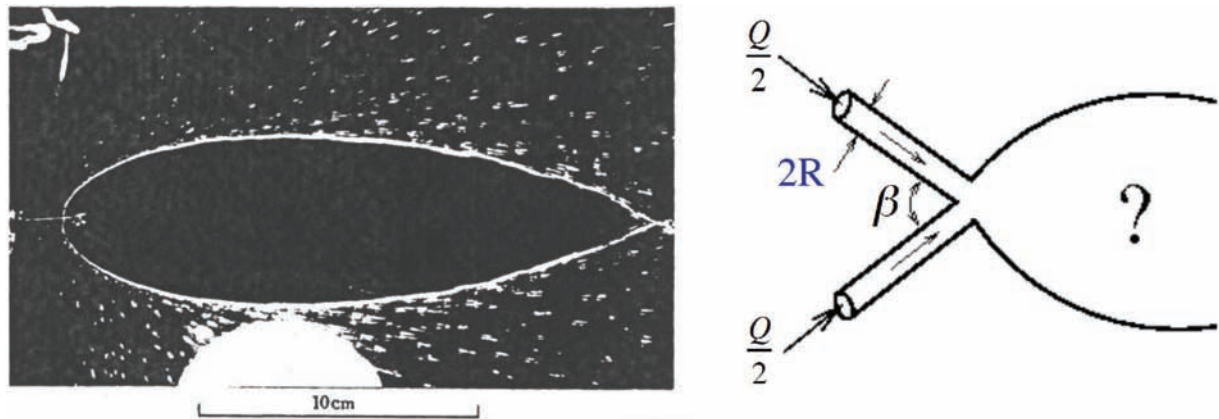


Figure 13.2: A sheet generated by the collision of water jets at left. The fluid streams radially outward in a thinning sheet; once the fluid reaches the sheet rim, it is ejected radially in the form of droplets. From *G.I. Taylor (1960)*.

We now consider the non-axisymmetric fluid , such as may be formed by the oblique collision of water jets (see Fig. 13.2), a geometry originally considered by *Taylor (1960)*. Fluid is ejected radially from the origin into a sheet with flux distribution given by $Q(\theta)$, so that the volume flux flowing into the sector between θ and $\theta + d\theta$ is $Q(\theta)d\theta$. As in the previous case of the circular sheet, the sheet rims are unstable, and fluid drops are continuously ejected therefrom. The sheet shape is computed in a similar manner, but now depends explicitly on the flux distribution within the sheet, $Q(\theta)$. The normal force balance on the sheet edge now depends on the normal component of the sheet speed, u_n :

$$\rho u_n^2(\theta)h(\theta) = 2\sigma \quad (13.7)$$

The sheet thickness is again prescribed by (13.5), but now $Q = Q(\theta)$, so the sheet radius $R(\theta)$ is given by the Taylor radius

$$R(\theta) = \frac{\rho u_n^2 Q(\theta)}{4\pi\sigma u} \quad (13.8)$$

Computing sheet shapes thus relies on either experimental measurement or theoretical prediction of the flux distribution $Q(\theta)$ within the sheet.

13.4 Lenticular sheets with stable rims

In a certain region of parameter space, specifically, with fluids more viscous than water, one may encounter fluid sheets with stable rims (see www-math.mit.edu/~bush/bones.html). The force balance describing the sheet shape must change accordingly. When rims are stable, fluid entering the rim proceeds along the rim. As a result, there is a centripetal force normal to the fluid rim associated with flow along the curved rim that must be considered in order to correctly predict the sheet shapes.



Figure 13.3: The “Fluid fishbone” formed by the collision of two jets of a glycerine-water solution. *Bush & Hasha (2004)*.

The relevant geometry is presented in Fig. 13.4. $r(\theta)$ is defined to be the distance from the origin to the rim centreline, and $u_n(\theta)$ and $u_t(\theta)$ the normal and tangential components of the fluid velocity in the sheet where it contacts the rim. $v(\theta)$ is defined to be the velocity of flow in the rim, $R(\theta)$ the rim radius, and $\Psi(\theta)$ the angle between the position vector \mathbf{r} and the local tangent to the rim centreline. Finally, $r_c(\theta)$ is defined to be the radius of curvature of the rim centreline, and s the arc length along the rim centreline. The differential equations governing the shape of a stable fluid rim bounding a fluid sheet may be deduced by consideration of conservation of mass in the rim and the local normal and tangential force balances at the rim.

For a steady sheet shape, continuity requires that the volume flux from the sheet balance the tangential gradient in volume flux along the rim:

$$0 = u_n h - \frac{\partial}{\partial s} (v \pi R^2) \quad (13.9)$$

The normal force balance requires that the curvature force associated with the rim's surface tension balance the force resulting from the normal flow into the rim from the fluid sheet and the centripetal force resulting from the flow along the curved rim:

$$\rho u_n^2 h + \frac{\rho \pi R^2 v^2}{r_c} = 2\sigma \quad (13.10)$$

Note that the force balance (13.7) appropriate for sheets with unstable rims is here augmented by the centripetal force. The tangential force balance at the rim requires a balance between tangential gradients in tangential momentum flux, tangential gradients in curvature pressure, viscous resistance to stretching of the rim, and the tangential momentum flux arriving from the sheet. For most applications involving high-speed sheets, the Reynolds number characterizing the rim dynamics is sufficiently large that viscous resistance may be safely neglected. Moreover, the curvature term $\nabla \cdot \hat{\mathbf{n}}$ generally depends on θ ; however, accurate to $O(R/r_c)$, we may use $\nabla \cdot \hat{\mathbf{n}} = 1/R$. One thus obtains:

$$\frac{\partial}{\partial s} (\pi R^2 v^2) = h u_t u_n - \frac{\pi R^2 \sigma}{\rho} \frac{\partial}{\partial s} \left(\frac{1}{R} \right). \quad (13.11)$$

Equations (13.9)-(13.11) must be supplemented by the continuity relation,

$$h(r, \theta) = \frac{Q(\theta)}{u_0 r} \quad (13.12)$$

in addition to a number of relations that follow directly from the system geometry:

$$u_n = u_0 \sin \Psi \quad , \quad u_T = u_0 \cos \Psi \quad , \quad \frac{1}{r_c} = \frac{\sin \Psi}{r} \left(\frac{\partial \Psi}{\partial \theta} + 1 \right) \quad (13.13)$$

The system of equations (13.9-13.13) may be nondimensionalized, and reduce to a set of coupled ordinary equations in the four variables $r(\theta)$, $v(\theta)$, $R(\theta)$ and $\Psi(\theta)$. Given a flux distribution, $Q(\theta)$, the system may be integrated to deduce the sheet shape.

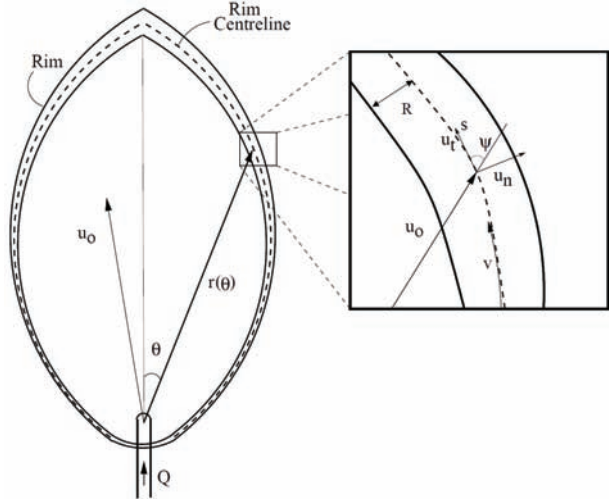


Figure 13.4: A schematic illustration of a fluid sheet bound by stable rims.

13.5 Water Bells

All of the fluid sheets considered thus far have been confined to a plane. In §13.1, we considered circular sheets generated from a vertical jet striking a horizontal impactor. The sheet remains planar only if the flow is sufficiently fast that the fluid reaches its Taylor radius before sagging substantially under the influence of gravity. Decreasing the flow rate will make this sagging more pronounced, and the sheet will no longer be planar. While one might expect the sheet to fall along a parabolic trajectory, the toroidal curvature of the bell induces curvature pressures that act to close the sheet. Consequently, the sheet may close upon itself, giving rise to a water bell, as illustrated in Fig. 13.5. A recent review of the dynamics of water bells has been written by *Clanet (Ann.Rev.)*. We proceed by outlining the theory required to compute the shapes of water bells.

We consider a fluid sheet extruded radially at a speed u_0 and subsequently sagging under the influence of a gravitational field $\mathbf{g} = -g\hat{\mathbf{z}}$. The inner and outer sheet surfaces are characterized by a constant surface tension σ . The sheet has constant density ρ and thickness $t(r, z)$. Q is the total volume flux in the sheet. The characteristic Re is assumed to be sufficiently high so that the influence of viscosity is negligible.

We define the origin to be the center of the impact plate; r and z are, respectively, the radial and vertical distances from the origin. u is the sheet speed, and ϕ the angle made between the sheet and the vertical. r_c is the local radius of curvature of a meridional line, and s the arc length along a meridional line measured from the origin. Finally, ΔP is the pressure difference between the outside and inside of the bell as may be altered experimentally.

Flux conservation requires that

$$Q = 2\pi r t u \quad (13.14)$$

while Bernoulli's Theorem indicates that

$$u^2 = u_0^2 + 2gz \quad (13.15)$$

The total curvature force acting normal to the bell surface is given by

$$2\sigma \nabla \cdot \mathbf{n} = 2\sigma \left(\frac{1}{r_c} + \frac{\cos \phi}{r} \right) \quad (13.16)$$

Note that the factor of two results from there being two free surfaces. The force balance normal to the sheet thus takes the form:

$$\frac{2\sigma}{r_c} + \frac{2\sigma \cos \phi}{r} - \Delta P + \rho g t \sin \phi - \frac{\rho t u^2}{r_c} = 0 \quad (13.17)$$

Equations (13.14), (13.15) and (13.17) may be appropriately nondimensionalized and integrated to determine the shape of the bell.

Note:

- the bell closes due to the out-of-plane curvature
- the influence of g is reflected in top-bottom asymmetry. Note that g is not significant in Fig. 13.5. The relevant control parameter is $\mathcal{F}r = \text{INERTIA}/\text{GRAVITY} = U^2/gL \sim 1$
- if deflected upwards by the impactor, the bell will also close due to σ

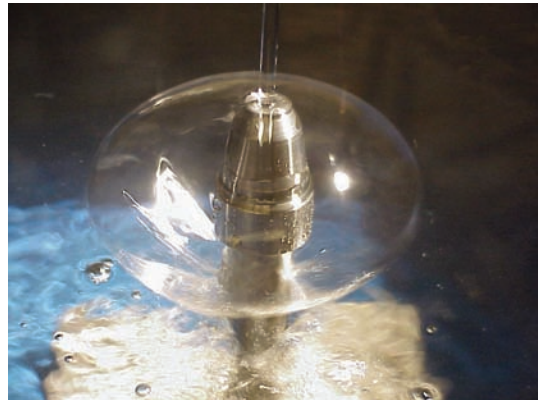


Figure 13.5: A water bell produced by the impact of a descending water jet on a solid impactor. The impactor radius is 1 cm. Fluid is splayed radially by the impact, then sags under the influence of gravity. The sheet may close on itself owing to the azimuthal curvature of the bell.

13.6 Swirling Water Bell

Consider the water bell formed with a swirling jet (*Bark et al. 1979*).

Observation: Swirling bells don't close. Why not?

Conservation of angular momentum: as r decreases, v increases as does $F_C \sim v^2/r$.

Sheet velocity:

$$\mathbf{v} = \underbrace{u\hat{e}_s}_{\text{in plane}} + \underbrace{v\hat{e}_\theta}_{\text{swirl}} \quad (13.18)$$

$$\text{Continuity: } Q = 2\pi rhu \quad (13.19)$$

$$\text{Conservation of Angular Momentum: } vr = v_0r_0 \quad (13.20)$$

$$\text{Energy conservation: } u^2 + v^2 = 2gz + u_0^2 + v_0^2 \quad (13.21)$$

$$\text{Normal force balance: } \frac{2\sigma}{R} + \frac{2\sigma \cos \phi}{r} + \rho gh \sin \phi = \Delta P + \frac{\rho hu^2}{R} + \frac{\rho hv^2 \cos \phi}{r} \quad (13.22)$$

Evidently, the bell fails to close owing to the influence of the centripetal forces induced by the swirl.

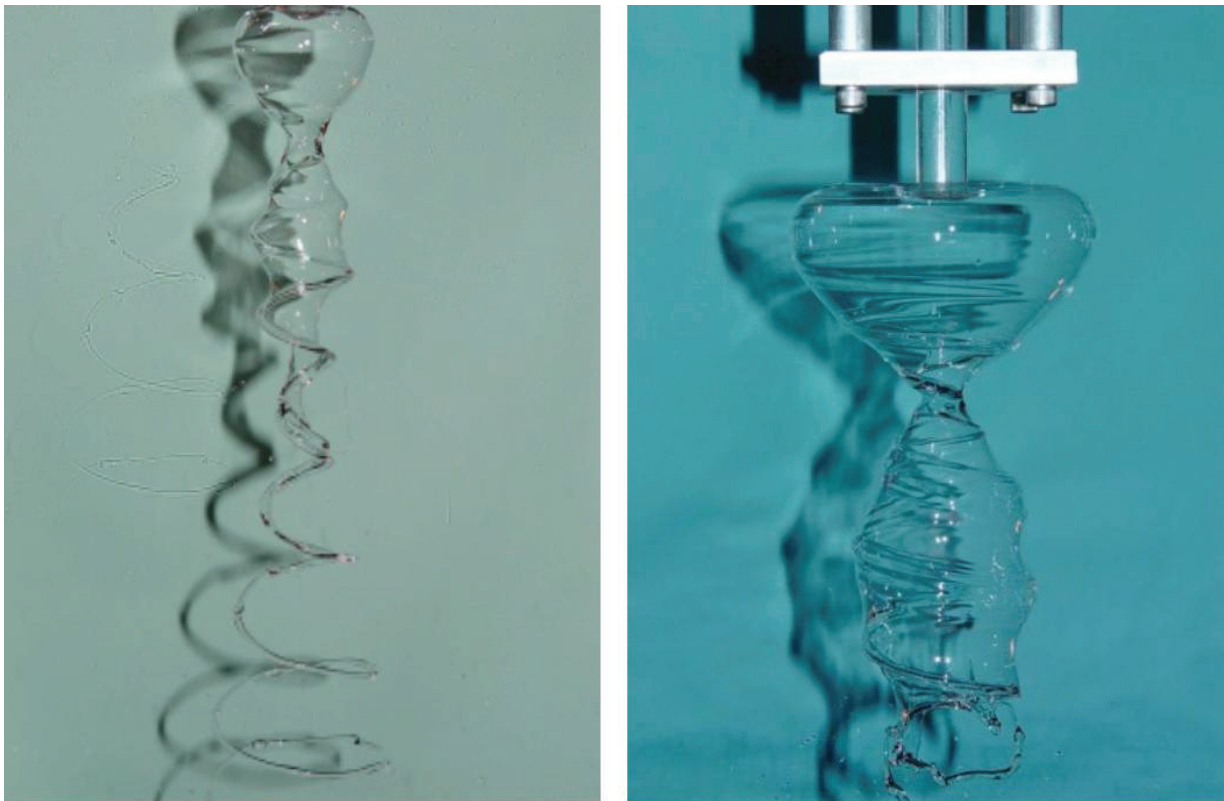


Figure 13.6: Swirling water bells extruded from a rotating nozzle.

MIT OpenCourseWare
<http://ocw.mit.edu>

357 Interfacial Phenomena
Fall 2010

For information about citing these materials or our Terms of Use, visit: <http://ocw.mit.edu/terms>.